

## Travel time distributions under convergent radial flow in heterogeneous formations: Insight from the analytical solution of a stratified model

Daniele Pedretti<sup>a,b</sup>, Aldo Fiori<sup>c</sup>

<sup>a</sup>GHS-UPC Hydrogeology Group, Department of Geotechnical Engineering and Geosciences, Universitat Politècnica de Catalunya, C/Jordi Girona 1-3, E08034 Barcelona, Spain

<sup>b</sup>University of British Columbia, Department of Earth and Ocean Sciences, 2207 Main Mall, Vancouver, BC V6T 1Z4, Canada

<sup>c</sup>Dipartimento di Ingegneria, Università degli Studi Roma Tre, Via V. Volterra, 62, 00146 Rome, Italy

### Abstract

We analyze conservative solute transport under convergent flow to a well in perfectly stratified porous media, in which the hydraulic conductivity is treated as a random spatial function along the vertical direction ( $K(z)$ ). The stratified model provides a rare exception of an exact analytical solution of travel time distributions in the proximity of pumping wells, and it is used here to obtain insights about ergodic and nonergodic transport conditions under nonuniform flow conditions. In addition, it provides a benchmark for numerical models aiming to correctly reproduce convergent flow transport in heterogeneous media, such as indicating the minimum number of layers required to obtain ergodic travel time distributions using only one model realization. The model provides important insights about the shape of the depth-integrated concentrations over time measured at the well (breakthrough curves, BTCs), which are usually applied to obtain transport parameters of the subsurface. It can be applied to any degree of system's heterogeneity and using either resident or flux-weighted injection modes. It can be built using different probabilistic distributions of  $K$ . In our analysis, we consider a log-normal  $K$  distribution, and the results indicate that, especially for highly heterogeneous systems, described by the log- $K$  variance ( $\sigma_K^2$ ), the minimum number of layers required for from one model simulation to reproduce ergodic travel time distributions can be prohibitively high, e.g., above  $10^6$  for  $\sigma_K^2 = 8$  considering flux-weighted injections. This issue poses serious concerns for numerical applications aiming to simulate transport in the proximity of pumping wells. In addition, this simple solution confirms that stratification can lead BTCs to display strong preferential flow and persistent, power-law-like late-time tailing. Since the latter are common phenomenological macroscale evidences of other microscale hydrodynamic processes than pure advection (e.g., mass-transfer), caution must be taken when inferring aquifer properties controlling the anomalous transport dynamics in heterogeneous media from BTCs fitting.

### Introduction

Predicting solute transport behavior for optimal aquifer risk assessment and remediation is a challenging and uncertain task. The presence of hydraulic heterogeneities, which involve erratic spatial distributions of hydraulic properties controlling transport in the subsurface (e.g., the hydraulic conductivity,  $K$ ) and the associated computational and technical difficulties, renders the spatio-temporal distribution of solute concentration amenable to be treated under a stochastic perspective [1]. Despite stochastic modeling in hydrogeology being a well-established discipline (e.g., [2-4]), there are still unexplored fields, such as the analysis of transport under radial convergent flow to a well, which require high attention for their practical utility.

Convergent flow is a very common configuration in groundwater applications. For instance, it applies under convergent flow tracer tests (CFTTs), which are routinely used to infer transport parameter and predict solute transport behavior in aquifers [5-10]. Despite their extended use, the interpretation of CFTTs is still problematic. For instance, obtaining information after breakthrough curve (BTC)

fitting is cumbersome because of the fundamental difference between radial and uniform flow transport, which can be a source of error if not accounted for [11]. Analytical stochastic solutions are rarely applicable as they are usually based on weakly heterogeneous conditions ( $s^2Y < 1$ , where  $s^2Y$  is the variance of  $Y = \ln K$ ) and under uniform flow conditions. Numerical modeling provides a robust alternative to deal with highly heterogeneous transport (e.g., [12-14]), but they need to cope with problems of convergence and other numerical issues (like, e.g., the number of particles in Lagrangian models and the spatio-temporal discretization in Eulerian approaches), which can limit their extensive use in practical application.

The system becomes further complicated when radial flow is used to characterize heterogeneous formations. Most of the traditional analytical stochastic solutions for mean uniform flow (e.g., [4]) cannot be applied under nonstationary conditions, which are intrinsic in the radial flow configuration [15]. Approximate solutions assuming low heterogeneity and high anisotropy of aquifers have been applied to describe divergent transport in Multi-Gaussian fields of  $Y$  [16-18]. However, such solutions cannot be applied in the case of convergent transport in highly heterogeneous formations.

Very few numerical approaches have been reported in the literature to address this issue (e.g., [19-21]). In most cases, modelers have to face large computational domains in order to ensure ergodic transport conditions in their simulations. All these aspects leave the analysis of CFTTs in highly heterogeneous fields still a wide open field for research, despite its great relevance for practical purposes.

The main objective of this paper is to illustrate and analyze an exact analytical solution to describe travel time distributions in a heterogeneous stratified formation under radial convergent flow. Stratified models provide a powerful conceptual modeling framework of transport in confined aquifers consisting of layered geological bodies or for transport in single fractures close to physical boundaries. Stratified models have been widely explored in the literature from different perspectives since the 1960s (e.g., [22-28]), even though the assumption of uniform flow conditions has been always considered. Stratified models provide exact analytical stochastic solutions for any degree of soil heterogeneity and type of  $K$  distributions. As shown in the following section, this can be easily shown also for convergent radial flow configurations.

This analysis serves to illustrate that this simple solution is able to show how the shape of the BTCs depends directly (a) on stratification and especially on vertical variability (heterogeneity) of the soil structure, (b) on the type of tracer injection, and (c) on the ergodic conditions where the solute travel time distributions are generated from, and that mainly depend upon the number of layers used for the aquifer discretization.

The first goal is to illustrate that a simple model based on a perfectly stratified radial flow configuration is able to generate anomalous travel time distributions (i.e., BTCs showing highly positively or negatively skewed travel time distributions) with similar features than those commonly observed on depth-integrated non-Fickian BTCs (i.e., non symmetric distributions of concentrations measured over time at a fixed controlling section) from field experiments. This similarity is of fundamental importance since commonly aquifer hydrodynamic properties are sometimes inferred from specific patterns on BTCs. It has been shown that the latter patterns depend directly on the conceptual and physical conceptual model used to simulate microscale aquifer structures. Examples include the spatial distribution of porosities [9], presence of inclusions (e.g., [29]), fractional derivative approaches to transport [30], mass-transfer processes (e.g., [31]), nonstationary correlation structures in multiGaussian stochastic models (e.g., [32]) or conditional connectivity [33]. A classic example is for instance the apparent power-law latetime scaling of BTCs, which has been sometimes observed in field experiments. In this case, several physical-based models can be used to fit the BTCs, such as those simulating diffusive-based mass-transfer mechanisms following a power-law memory function (e.g., [31]). However, there are other mechanisms leading to power-law-shaped BTCs. Pedretti et al. [21], using 3D numerical simulations based

on unconditional multiGaussian fields, showed that under convergent radial flow configurations the late-time behaviors on BTCs can scale as a power-law function because of the underlying stratified flow distributions. Contrarily to Pedretti et al. [21], in this work we explicitly start from an analytical solution based on a stratification conceptual model to illustrate the relationship between stratification and anomalous BTCs under a radial convergent flow configuration.

A second goal is that this analytical model indicates the conditions for which incomplete sampling occurs, e.g., when the injection well is not fully penetrating or is screened over a limited subset of the stratified medium. Such conditions may lead to nonergodic transport, for which the BTC is subject to uncertainty. We better define the concept of ergodicity later in the text.

In this same line, the third goal is to show that this model can be used as a benchmark for numerical simulations aiming at reproducing radial convergent transport in highly heterogeneous media, emphasizing possible problems related to incomplete sampling or numerical deficiencies in handling strong K contrasts. It suggests the minimum required resolution (in terms of number of layers) that a simulation requires to adequately reproduce the impact of the underlying heterogeneous soil structure on the BTCs.

The paper is structured as follows. We first describe the conceptual model (Section 2.1), the mathematical derivation of the travel time distributions (Section 2.2) and their analytical solutions using a log-normal distribution of the hydraulic conductivity in terms of resident or flux-weighted injection modes. The results are presented in the following manner: first, the ergodic case of travel time distributions, depending on the type of injection (Section 3.1). Afterwards, we analyze the nonergodic case, involving the limited sampling of K (Section 3.2). We also evaluate here the global errors between analytical and numerical results depending on the degree of subsampling. Finally, the paper concludes with a discussion and the main conclusions drawn from this work.

## 2. Methodology

### 2.1. Conceptual model

A conceptual sketch of the aquifer configuration is depicted in Fig. 1. We consider a formation characterized by thickness  $b$  (constant in space) and divided into a number of layers  $NL$ . All layers are characterized by the same constant thickness  $L$ , proportional to the vertical integral scale of  $K$ , such that  $L_i = b/NL$ , where  $i$  ( $i=1, \dots, NL$ ) indicates the generic layer of the formation. The formation is perfectly stratified, meaning that the hydraulic conductivity  $K$  is homogenous in each of the layer composing the formation, but heterogeneous along the vertical axis ( $K=K(z)$ ). We treat  $K(z)$  as a stationary random function, with given univariate distribution  $f(K)$ .

The stratified formation is very useful in grasping the main features of transport in heterogeneous media, leading to an exact solution for flow and transport; for this reason it has been employed in the past, although mainly for transport under mean uniform flow. Such a conceptual model may also be adopted to model flow and transport in more realistic three-dimensional formations, provided that the solute is injected at a close distance from the pumping well, say at distances of the order of the horizontal integral scale of  $K$  (e.g., [2,21]).

To simulate transport in a CFTTs scheme, we account for an extraction well with radius  $r_w$  and a passive well at a radial distance  $r_0$  from it. The pumping well is fully penetrating and screened along the full aquifer, while the passive well may sample a more limited section of the porous medium. The extracting well is discharging for sufficient time at a constant rate  $Q$  to generate steady-state conditions at the passive well area.

An injection of a conservative solute of total mass  $M$  takes place as a pulse injection from the passive well, acting as an injection line. Local dispersion and diffusion mechanisms are not accounted for; as such, solute exclusively moves due to

advection. In this sense, BTCs describing the distribution of solute flux at a controlling section over time can be modeled within a Lagrangian framework assuming travel time distributions of solute particles moving from the injection to the extraction well. Note that the incorporation of dispersive mechanisms is not possible in this analytical solution, but it can be readily performed from a numerical perspective (e.g., using a particle tracking approach [13,21]).

Injection modes are usually modeled in terms of residence or flux-weighted concentration [34,35]. Past work shows how the selection of this boundary condition controls the spatio-temporal behavior of solute plumes, with direct consequences on transport parameter estimation and on the physical mechanisms such as mixing and spreading (e.g., [36–38]). The reason is qualitatively explained in Fig. 1. At the top of this figure (Fig. 1a), in case of 'resident' injection (R), solute particles are equivalently distributed at the injection line at the initial time ( $t_0$ , red particles). As soon as the particles are released, they start travelling along the layer as in a confined stream tube, at a radially increasing velocity towards the well. Because layers do not exchange mass, solute particles remain constrained between the injection and the limit of the extraction well, where they finally mix with the other particles in the well column. Solute particles move depending on the mean tube velocity; at the snapshot time  $t_3$ , solutes have already travelled along the most conductive channel (white), so that the mass moving in this channel has been extracted from the well and collected at the surface.

No mixing mechanisms between layers also occur in case of FW injection (Fig. 1b); however, in this case the mass entering each layer from the injection line is proportional to the layer's  $K$ . This is done aiming at reproducing the preferential distribution of the solute in the domain at the different depths because of the imperfect mixing condition in the passive well at the beginning of the test. Because of this weighting mechanism, most of the mass is injected in the higher channel; as such, more mass is collected earlier in FW injection mode than in R injection mode. The mathematical formulation of travel time distributions for this model and the different types of injections is described hereafter.

## 2.2. Travel time analysis

We analyze here the travel time distributions to the pumping well assuming the conceptual model illustrated above. The problem can be stated in a radial coordinates framework; we therefore define the transposed vector  $(r, z)^T$ , where  $r$  is the plane (radial) direction and  $z$  is the vertical direction. We impose that the piezometric head at the well and at a distance  $R$  from it are constant along the vertical, with  $h_w$  the head at the well. This way, the system behaves as a parallel series of resistors, the piezometric head  $h$  being constant along  $z$  and variable along  $r$  ( $h=h(r)$ ); thus, no water flux exists between the layers. Under the above conditions, the Thiem solution [39] applies for each layer, and the head at each layer  $h_i$  is equal to

(1)

$$h_i(r) - h_w = \frac{q_i N_L}{2\pi K_i b} \ln \frac{r}{r_w}$$

where  $q_i$  is the specific discharge in the  $i$ -th layer. To accomplish for the head boundary condition it must be also accomplished that  $q_i = AK_i$ , where the constant  $A$  is found by prescribing that the total discharge rate is  $Q$  at the well location [40,41], as follows

(2)

$$Q = \sum_{i=1}^{N_L} q_i = A \sum_{i=1}^{N_L} K_i \Rightarrow A = \frac{Q}{N_L \bar{K}}$$

where  $\bar{K}$  is the arithmetic mean of  $K$ . In each layer, the solute velocity is given by

(3)

$$v_i(r) = \frac{K}{\phi} \frac{\partial h_i}{\partial r} = \frac{K_i}{\bar{K}} \frac{Q}{2\pi b \phi r}$$

where  $\phi$  is the porosity (assumed as constant). Note that the velocity depends on the distance  $r$  from the extraction well. The travel time for each layer  $t_i$  is obtained integrating Eq. (3) with respect to  $r$  such that

(4)

$$t_i = \int \frac{dr}{v_i(r)} = \frac{\pi b \phi \bar{K} (r^2 - r_w^2)}{Q K_i}$$

The problem can be cast in dimensionless variables, working with the random variable  $\tau_i$  (following e.g., [42])

(5)

$$\tau_i = \frac{Q t}{\pi b \phi (r^2 - r_w^2)} = \frac{\bar{K}}{K_i}$$

In the limit case of one layer ( $N_L=1$ ) (homogeneous formation),  $\bar{K}=K_i$  and the travel time is constant and deterministic ( $\tau_i=1$ ). Conversely, when the number of layers is very large ( $N_L \gg 1$ ),  $\bar{K} \rightarrow K_A$ , where  $K_A$  is the ensemble arithmetic mean of  $K_i$ , and  $\tau_i = K_A / K_i$ .

We define the latter case as our reference, or ‘‘ergodic’’, conditions, for which the entire distribution of  $K$  is sampled by the monitoring system. Intermediate cases belong to ‘‘non-ergodic’’ conditions. We refer to ergodicity in this paper, thus, as the possibility that the model is sufficiently detailed, in terms of vertical discretization, that its results from the adoption of any random  $K$  distributions (following the same probabilistic function) do not depend on the number of layers used to run the simulations. This also means that any adopted spatial organization - along the vertical direction - of the  $K$  value from the same population does not influence the resulting BTCs. It should be remarked that field-based depth-integrated BTCs are not necessarily an indication of ergodic transport in real aquifers. In a numerical framework, however, establishing ergodic transport conditions is particularly useful for benchmarking purposes, as they allow evaluating possible departure from well-defined reference conditions due to aquifer subsampling. These concepts are further elaborated in the following sections.

### 2.3. Ergodic transport

Under the 'ergodic' assumption, the number of layers is large enough to sample the entire distribution of  $K$ . Hence,  $\bar{K} = \langle K \rangle = K_A$ , the arithmetic mean, and from (5) it is  $\tau_i = K_A/K_i$ , and the travel time is inverse proportional to the hydraulic conductivity.

The lognormal distribution is a suitable model to describe the distribution of  $K$  in stochastic subsurface hydrology [43]. With  $Y = \ln K$  the log-conductivity, the lognormal distribution is fully characterized by the mean  $\langle Y \rangle = \ln K_G$ , with  $K_G$  the geometric mean of  $K$ , and the log-conductivity variance  $\sigma_Y^2$ . Notice that lognormal distributions are self-replicating under multiplication and division or multiplication by a constant. This means that the products and quotients of log-normal random variables are themselves log-normal distributions [44,45]. Thus, since  $K_i$  is lognormal, so is  $\tau_i$ . This has an important implication in the interpretation of BTCs, as pointed out in the next sections. Hence, applying Eq. (5) and using our previous definition  $Y = \ln(K)$ , the travel time probability density function (PDF) can be written as follows:

(6)

$$f_R(\tau) = \frac{1}{\tau \sqrt{2\pi\sigma_Y^2}} \exp \left[ -\frac{(\ln \tau - \sigma_Y^2/2)^2}{2\sigma_Y^2} \right]$$

As shown in the sequel, the above travel time distribution is equivalent to the BTC for a resident concentration injection condition, hence the subscript R. Note that the selection of a log-normal  $K$  distribution in a perfectly stratified media where all the layers are of the same thickness leads to a linear type of correlation covariance between strata (e.g., [2]) where the integral scale is half the thickness of each layer. For this reason, we indistinctively refer in this text either to layer sampling or to integral sampling in the following pages.

In a Lagrangian framework, there is a strict relationship between the travel time distributions and the solute masses distribution at a controlling section [4, p. 166]. Consider the injected mass  $M$  as a bundle of particles  $N_p$ , each of them carrying the same amount of mass ( $m_p = N_p/M$ ). Because there is no transversal dispersion, we can assume in our model that one single particle per layer is representative of the travel time occurring in that specific layer. The total mass can be divided by the number of layers such that  $N_p = N_L$ . Thus, the mass distribution after a certain time is given by the number of particles arriving at a controlling section at a specific time. Such relationship depends however on the way solutes are released at the beginning of the tracer tests from a passive well. As discussed above, two general types of boundary conditions are generally accepted: resident (R) or flux-weighted (FW) injection modes.

If R injection mode is used, it is assumed that the mass is initially ( $t=0+$ ) homogeneously distributed along the vertical column of the injection well. Translated to our model, we can assume that particle is located in each layer at  $t=0+$ . In this sense, the analytical solutions for travel time PDF for the resident injection is Eq. (6) for the lognormal  $K$  distribution, which we shall denote in the following as  $f_R(\tau)$ .

Matters are different for the flux weighted (FW) injection mode, which is more realistic than the resident mode in real applications. The mass of contaminant entering the domain at  $t=0+$  is controlled preferentially by the local flow velocities which are encountered at different depths from the heterogeneous topsoil. Considering a constant mean gradient between the injection and extraction well, it means that the injected mass at different depths is weighted by the local value of  $K$ , i.e.,  $m_{p,i} \propto K_i$ . Because in our stratified model  $K_i \propto \tau^{-1}$ , the travel time PDF for the flux-weighted (FW) injection mode is simply related to the one using resident injections by

(7)

$$f_{FW}(\tau) = \frac{f_R(\tau)}{\tau}$$

where the subscripts indicate the type of injection considered.

Thus, Eqs. (6) and (7) completely describe the BTC for the resident and flux-weighted injection conditions, respectively. It is easy to ascertain that the first two moments of the travel time distributions are given by the following expressions

$$\begin{aligned} \langle \tau \rangle &= \exp(\sigma_Y^2) \quad (R); \quad \langle \tau \rangle = 1 \quad (FW), \\ \sigma_\tau^2 &= \exp(2\sigma_Y^2)(\exp(\sigma_Y^2) - 1) \quad (R); \quad \sigma_\tau^2 = \exp(\sigma_Y^2) - 1 \quad (FW). \end{aligned}$$

It is seen that the travel time variance is not linear dependent on the distance, being  $\sigma_Y^2 \propto (r^2 - r_w^2)^2$ . hence, transport is anomalous for the present setup [46].

#### 2.4. Nonergodic transport

Analyzing the situation where the number of layers is not large enough to accomplish the ergodic conditions is important for two main reasons. First of all, in practical situations wells are drilled to explore a limited number of layers of a heterogeneous domain. In other words, the wells sample only a limited number of vertical integral scales characterizing the spatial distribution of  $K$ . A common situation is to count on tens to hundreds of vertical integral scales, with rare exceptions of thousands of samples (e.g., [47]). In the case that the finite number  $NL$  of hydraulic conductivity samples is not sufficient to ensure a clear picture of the actual distribution of  $K$ , transport could be modeled under 'nonergodic' conditions. Secondly, a similar situation might occur in 3D numerical simulations, in which the memory and CPU constraints impose a limited vertical size of the flow domain and/or a limited number of random simulations, in stochastic frameworks. In all those cases the analytical solutions for the travel time distributions presented above would be no longer valid, as they imply a complete sampling of the  $K$  distribution. The travel time PDF for the nonergodic case defies an analytical solution, and the calculation of the travel time PDF is carried out numerically along the following procedure.

We therefore analyze in detail what occur when ergodic conditions are not fulfilled, by generating (random) sets of  $K_i$  values, with  $NL \ll \infty$ ; the related  $\tau_i$  distributions are obtained using Eq. (5). Then the  $\tau_i$  are sorted, from the smallest to the highest values. In the case of resident (R) injections, the experimental discrete CDF values  $CR$  is a vector of length  $NL$ , the generic value  $CR_j$  being equal to  $j/NL$ . That is, in the resident injection mode all the particles have the same mass. For the FW type of injection, an additional step is needed. From the sorted vector  $\tau_j$ , we generate a vector of weights  $p_j$  which reflect the mass attached to each particle.  $p_j$  is a function of the local velocity of the  $j$  stratum, which is in turn proportional to  $K_j$ . Hence, the weight employed in the calculations is equal to

(8)

$$p_j = \frac{K_j}{K} = \frac{1}{\tau_j}$$

We highlight that  $K_j$ , following the same index of the sorted vector  $s_j$ , goes from the higher to the smaller values, since  $\tau \propto K^{-1}$ . With such weights  $p_j$ , we generate the experimental CDF for the FW injection mode,  $CFW$ , as

(9)

$$C_j^{FW} = \frac{1}{N_L} \sum_{k=1}^j p_k$$

### 3. Results and discussion

We report and discuss in this section the main results of our analysis. We first analyze the ergodic case, which helps analyze the ensemble behavior of the stratified model depending on the degree of variability of  $K$ . This is useful to further explore what occurs in nonergodic conditions, so as to compare the latter behavior with the analytical solutions and to have a quantitative measurement about the departure from ergodic conditions.

#### 3.1. Ergodic case

In Fig. 2 we plot the travel time PDFs as a function of dimensionless travel time  $s$  for the two injection modes considered (Eqs. (6) and (7)), for different distributions of  $Y = \ln K$ , assuming ergodic conditions. Considering the high variability of the distributions, we have reproduced in the inserts the travel time PDF in log scales. For the sake of further comparisons with the nonergodic case (carried out in the next section) we also reproduce in Fig. 3 the cumulative BTCs for the same cases of Fig. 2.

Several relevant aspects can be observed in the figure. First, the shape of the BTCs may be strongly nonsymmetric, as a function of the heterogeneity (epitomized by  $\sigma_Y^2$ ) and the type of injection. For very low heterogeneity ( $\sigma_Y^2 < 0.1$ ), the BTCs shape is rather symmetric for both types of injections and similar to the standard Inverse-Gaussian distribution, the peak of the BTC being around  $\tau = 1$ . In such conditions the injection mode does not have a significant influence on the BTC. As the variance increases, the peak of the BTC tends to depart from  $\tau = 1$  and the curve exhibits an increasing asymmetry. Also, the differences observed for the two injection modes start to be significant as  $\sigma_Y^2$  increases. In particular, when  $\sigma_Y^2 = 1$  (mild heterogeneity) the effect of the flux-weighted injection mode is dramatic as the BTC peak has sensibly moved toward low values of  $s$ . However, both R and FW show very long tailed distributions, which cannot be typically reproduced employing the Gaussian ADE model. A similar, anomalous behavior for transport was also found in stratified formations under uniform head gradients [24].

When the heterogeneity is very high ( $\sigma_Y^2 > 4$ ) the BTC becomes very skewed, the peak being hardly visible on the plots in arithmetic scales. In such cases, the injection mode plays a very important role in determining the overall shape of the BTC. One can observe from Fig. 2 that for  $\sigma_Y^2 = 8$  in the R injection mode, the peak of the BTC is found at  $\tau = 10^{-2}$ , i.e., strongly retarded as compared with the FW injection mode. In turn, the FW mode generally increases the mass of the fast arrivals. The damping effect caused by the resident injection model and the fast transport determined by the FW one acts as a warning against accurate selections of the boundary conditions in numerical simulations or analytical models involving solute transport under convergent flow.

Thus, the travel time PDFs (or the BTC) pertaining to transport in highly heterogeneous stratified media is characterized by a strong early mass arrival, which is due to high velocity preferential flow, and a long and persistent tailing. Such features have a significant impact in applications, like, e.g., those involving risk assessment or remediation (e.g., [48,49]). As for the latter, the slow arrivals of solute may indeed harm the effectiveness of a pump-and-treat remediation procedure. To further analyze the BTC tailing, we plot in Fig. 4 the distribution of travel time built with  $\sigma_Y^2 > 1$  in double log scales. This is a usual representation of BTCs from experiments, for instance to obtain effective transport models (e.g., [31]); in particular, power-law distributions of the BTC would appear as straight lines on these diagnostic plots. It is noticeable that the stratified model could

indicate apparent power-law distributions at late-time (i.e., after the peak), but this is only an apparent behavior which is pertinent to lognormal distribution with high variances. Specifically in Fig. 4 on the insert we report the local derivative  $\log(C)/\log(\tau)$ , sometimes called the power-law slope

' $m$ ', against  $\log(\tau)$ ,  $C$  being the travel time PDF. Notice that as the variance increases,  $m$  tends to around  $m=1$  which persist over time. In particular, for  $\sigma_Y^2 = 4$  and 8,  $m$  tends to values which are usually observed from field scale experiments under convergent flow i.e., of the order of  $m = 1$  to  $m = 3$  (e.g., [31]). This apparent power-law effect on the tails of log-normally distributed data is well known (e.g., [50]) but it can lead to misleading conclusions if a model fitting attempt is done only after partial knowledge of the entire behavior of the PDFs. With rare exceptions (e.g., [51]), BTCs are never collected over time intervals spanning more than 2-3 log time intervals; as such, care must be taken not to confuse stratifications with other kinds of mechanisms leading to a similar behavior (like, e.g., mass transfer into immobile zones), especially in the proximity of pumping wells (e.g., [21]).

All these effects on the early peak and the late-time behavior of the BTC have been observed under ergodic distributions of  $K$ . In most practical applications,  $K$  samples are never sufficient to obtain a clear picture of the entire heterogeneous structure. These aspects are analyzed in detail in the following section.

### 3.2. Nonergodic case

We explore here what happens when  $K$  is not completely sampled and transport takes place under nonergodic conditions. Because of the incomplete sampling, the travel time PDF is different for any realization of the  $K$  field, and here we aim to analyze (1) how the shape of the travel time distributions changes as a function of the  $K$  (i.e., the number of layers) sampled by the passive well, (2) the minimum number of layers required to obtain convergence of the numerical solutions towards ergodic results, and (3) an estimate of the variability of the travel time distributions within the realizations.

Since the transformation of cumulative distribution into densities is plagued with difficulties in most cases (e.g., [52]), we prefer here to display values in terms of CDFs, rather than using estimated PDFs, given such transformation not strictly necessary with the scope of this paper.

We analyze the nonergodic travel time CDF through a Monte Carlo approach, in which the statistics of the CDF are obtained after running and averaging the results of several random realizations. We therefore generate a constant number of realization  $N_R = 10^3$  of a random  $K$  field of  $NL$  layers and determine the ensemble statistics for the travel time CDF. The ensemble mean is found after first interpolating all the single realizations to a common discrete time scale and afterwards averaging all the CDF values for each time step. Note that the number of realization chosen here is arbitrary and done only for illustrative purposes. We could, for instance, have totally avoided a Monte Carlo scheme and used only one simulation having an additional number of layers (of the order of  $N_R$ ); however, our aim here it to stress the reader attention on the importance that the subsampling effect can have to obtain accurate model results with reference to the ergodic case, even in a Monte Carlo framework.

We begin with the ensemble mean of the CDF, and Fig. 5 reports the results of ensemble mean behavior for the different cases analyzed in this paper (increasing variance from the top to the bottom, and different injection modes). Note that in this figure all the plots show different horizontal log scales, as the variability of  $\tau$  depends on  $\sigma_Y^2$ , as shown in the previous analysis. For graphical purposes, we have plotted the curves referring to four different numbers of layers ( $NL = 2, 10, 100, 1000$ ). The CDF for  $NL = 1$  is always equal to  $H(\tau-1)$ , with  $H$  the Heaviside function. Starting from the top in Fig. 5, the case with lower heterogeneity ( $\sigma_Y^2 = 0.1$ ) indicates that a reduced number of layer such as  $NL = 10$ , which is a common and feasible vertical discretization in typical modeling approaches, satisfactorily

reproduces the ergodic, analytical solution (gray line underlying the plots). This is true for both the R-type and FW-type of injections. It should be noticed that NL=10 is possibly a minimum number of layers to be used in simulations for an accurate reproduction of transport under such a low variance. Using less layers, such as NL=2 (blue lines), leads to a significant departure from the ergodic case.

These conclusions are also valid also for  $\sigma_Y^2=1$ , even though the green dotted line representing NL=10 does not completely capture the system behavior, while a higher number of layers, such as NL=100 leads to a solution closer to the ergodic one. When the variance further increases to  $\sigma_Y^2=4$ , the differences appear much more evident and the effects of the type of injection also become important. For R-mode injections, the ensemble mean curve for NL= 10 dramatically departs from the ergodic case, while the CDF for the larger NL =100 is closer to the ergodic solution. This is no longer true for FW-type, and especially at early times. Such a larger dataset is also poorly reproducing the actual system behavior, as a consequence of how the experimental CDF in the case of flux-weighted injections is estimated (Eq. (9)). As explained there, for high values of  $\sigma_Y^2$ , the incomplete sampling mainly affects the high K values, so that the weights used to estimate the CDFs are not accurately reproduced. This effect is more visible for  $\sigma_Y^2=8$ . For both types of injections a minimum number of layers of NL=10<sup>3</sup> seems to be required, even though for FW-type injections the early-time behavior is not still completely captured, despite the large combination of layers and realizations. We highlight that if only one realization is adopted instead of a Monte Carlo framework, then one should opt for an unfeasible number of layers (around 10<sup>6</sup>) to obtain ergodic conditions; such a highly refined discretization can be of serious concern for the computation limitation of traditional computational machines.

As previously stated, the nonergodic CDF may change from realization to realization, as a function of the number of strata NL detected by the passive well, the heterogeneity and the injection mode. A global indicator of the uncertainty associated with the BTC is provided by the root mean square error (RMSE), which is a measure of the global difference between the ensemble mean and the random cumulative BTCs (i.e., the CDFs) provided by the numerical Monte Carlo solutions. The smaller the RMSE indicator, the closer the CDFs becomes to the ensemble solution. Denoting the ensemble CDF as  $f^E = \langle CDF_i \rangle$  and the CDF pertaining to the generic i-realization as  $f_i$ , the RMSE indicator can be formally written as

(10)

$$\text{RMSE}(N_L) = \sqrt{\frac{1}{n} \sum_{i=1}^n (f_i - f_i^E)^2},$$

where n is the total number data. Results are plotted in Fig. 6 in log scale, for  $\sigma_Y^2= 0.1, 1, 4, 8$  and for the two injection modes. The plots suggest that, for all cases, RMSE decays to zero for increasing NL; the behavior is expected as for NL  $\rightarrow \infty$  the CDF pertaining to each realization converges toward the ensemble result, leading to  $\text{RMSE} \rightarrow 0$ . While the convergence of the error to zero is relatively fast for low heterogeneity, it is much slower for increasing  $\sigma_Y^2$ , with significant differences between the two injection modes. As an example, the number of layers required to get a prescribed  $\text{RMSE}=10^2$  would be around 10<sup>2</sup> for the smaller  $\sigma_Y^2$  and several orders of magnitude larger for the higher  $\sigma_Y^2$ .

The above behavior has consequences on both numerical simulations and field applications dealing with high heterogeneity in which the number of vertical integral scales (i.e., layers) sampled by the solute is limited. In such cases, the CDF (or analogously the BTC) may be quite different from its ensemble counterpart, and a more detailed mapping of the K field in the region would be needed in order to reproduce correctly the experimental distributions. Also, these results are a warning against three-dimensional numerical solutions aiming to reproduce ergodic transport behavior, especially in the vicinity of the pumping well. Since computational times can dramatically increase with a large number of layers,

modelers may be sometimes tempted to make coarser vertical discretization in order to reduce the computation costs. However, these results show that in case of high variance, transport conditions similar to ergodic or ensemble ones can be reached only if a very large number of layers is employed. In other words, employing a limited number of vertical integral scales of  $K$  may lead to different travel time distributions for different realizations of the  $K$  field.

This issue also poses serious limitations also on the use of stochastic approaches aiming at simulating CFTTs, and especially on the ability of single realizations to reproduce ergodic transport. While this approach based on random realizations of the  $K$  field can be effectively used to understand important phenomena occurring in the proximity of wells (e.g., [21]), exporting general conclusions in a stochastic sense would be obtained only under a numerical setup that can be prohibitively large for practical purposes.

#### 4. Conclusions

An analytical solution of transport in heterogeneous media under radial convergent flow has been developed and employed to get insights on the breakthrough curve (BTC) of passive solutes. The model can be employed to simulate solute transport in the vicinity of pumping wells and in all those situations where the aquifer can be modeled as a perfectly stratified formation, with vertical distribution of hydraulic conductivity. The model is valid for any heterogeneity and distribution of the hydraulic conductivity  $K$ , and it may provide a useful benchmark solution for numerical models aiming at reproducing ergodic transport under radial convergent flow.

The main conclusions that can be drawn from this work are listed as follows:

We have developed and applied the stratified model to explore the behavior of solute when  $K$  is log-normally distributed, a common hypothesis in stochastic modeling. The results suggest that the travel time distributions are largely conditioned by the total system's heterogeneity, expressed in term of variance of log transformed  $K$ . In particular, when heterogeneity is strong the BTC is highly asymmetric and typically characterized by early arrivals, due to high-velocity preferential flow, and a persistent tailing, pertaining to the late arrivals of solute parcels, moving slowly in low-conductive regions;

The injection mode (resident or flux averaged) plays a key role in determining the BTC asymmetry: flux-weighted injections generally increase the mass which is delivered to the well in short times, while resident injections give a larger mass arrival at later times; these findings have important consequences for practical applications, like, e.g., risk assessment or aquifer remediation.

Apparent power-law behavior can be observed in the BTC when in presence of highly heterogeneous formations. There are other physical processes which may lead to power-law tailing, like, e.g., the presence of multiple rate mass transfer in "immobile" regions [31]. Hence, the apparent power-law behavior may lead to misleading conclusions regarding the conceptual and physical interpretation of the transport processes. This results is in agreement with the analysis by Pedretti et al. [21], which indicate transport stratification as the responsible of power-law behaviors in heterogeneous Multi-Gaussian fields.

When the  $K$  sampling operated by the solute plume is limited, e.g., when the passive well screens a relatively small number of layers (a condition usually met in real experiments), transport can become strongly non ergodic. In particular, a very large number of layers is needed to adequately sample the entire  $K$  distribution when  $\sigma_Y^2$  is large (strong heterogeneity). Also, the BTC may vary considerably as a function of the particular  $K$  realization adopted. Thus, field experiments in highly heterogeneous formations in which a limited subset of  $K$  is sampled can be characterized by a BTC very much different from the ergodic one. Similar behavior is expected for three-dimensional numerical simulations in which the vertical extent of the domain is not sufficient for an accurate sampling of the  $K$  field, e.g., to limit the computational burden of the simulation.

We highlight that our analysis is valid for transport in perfectly stratified formations, which usually takes place only in the proximity of pumping wells, although there might be specific geological conditions (e.g., lacustrine environments, fractures, etc.) for which the perfectly stratified formation is a suitable conceptual model for the K structure. Nonetheless, this analysis indicates significant features of transport under convergence flow in heterogeneous media, like, e.g., the strong asymmetric shape of the BTC, the fast, preferential flow and the persistent tailing, similar to power-law. Also, the analysis shows how problematic the actual reconstruction of convergent flow transport can be due to the nonergodic effects caused by incomplete sampling, which certainly need to be further explored due to its wide use for practical applications, like, e.g., convergent flow tracer tests (CFTTs).

List of figures

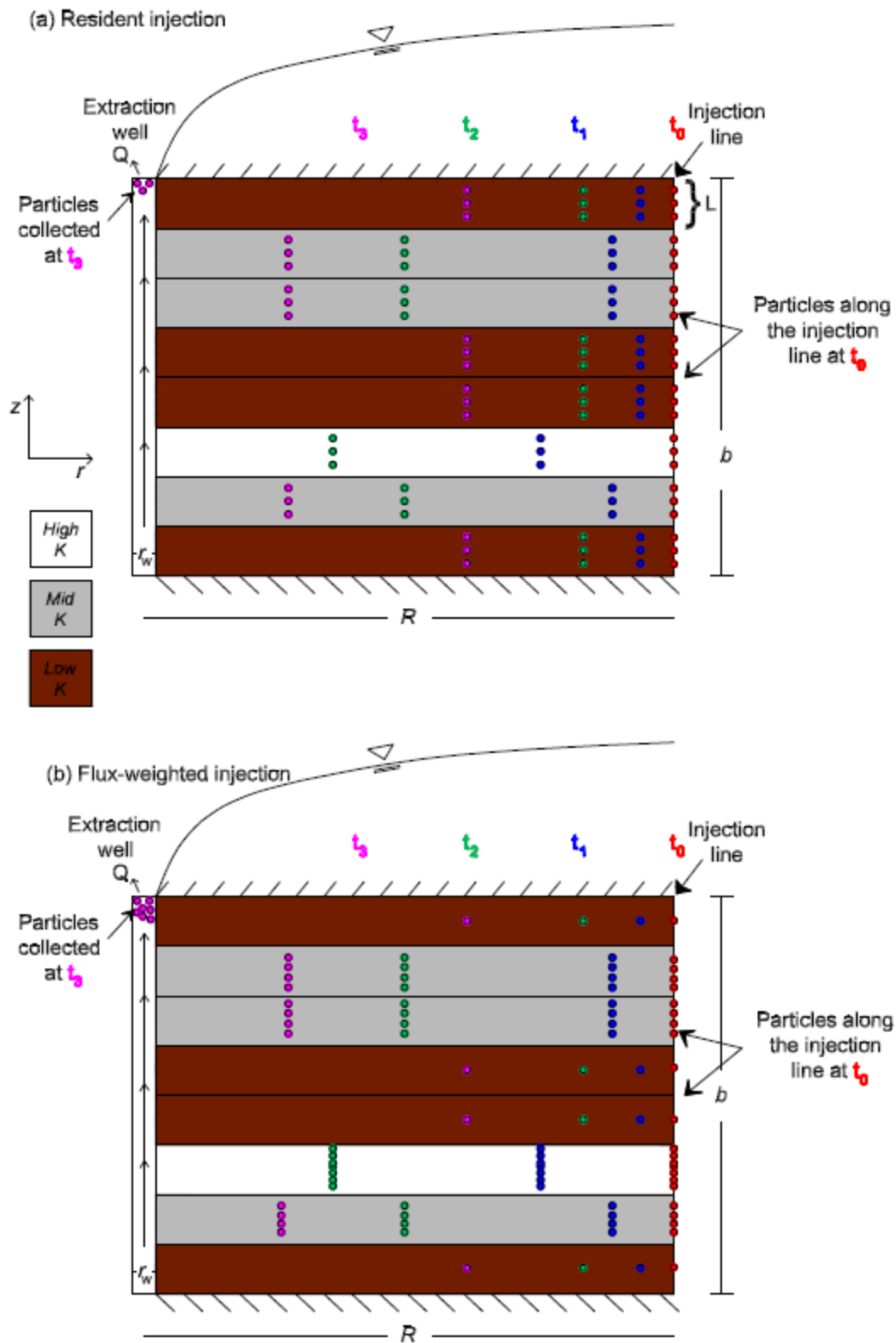


Fig. 1. Conceptual model of the stratified transport model.

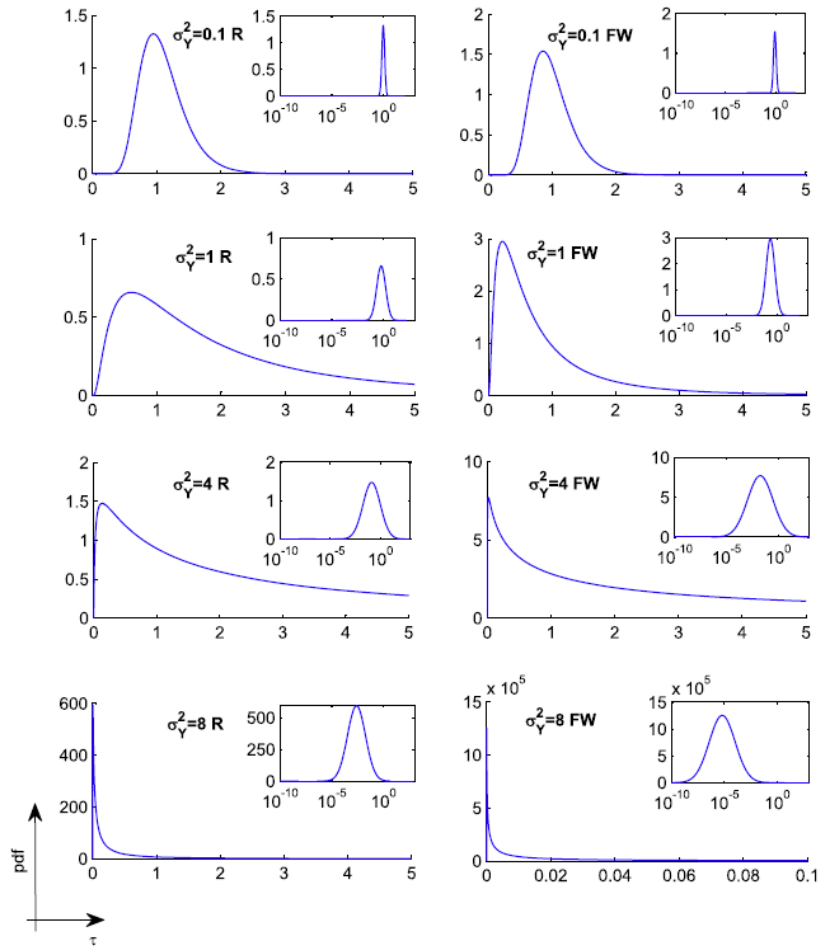


Fig. 2. Travel time probability density functions (*pdf*) for various  $\sigma_Y^2$  versus dimensionless time  $\tau$ , for resident (R) or flux-weighted (FW) injection modes in the ergodic case. The use of arithmetic scales is done to emphasize the dependence of the non-symmetric distributions with the variance and type of injection. Notice that because of the very large temporal spreading for the case  $\sigma_Y^2 = 8$ -FW, the horizontal axis of this plot is limited to  $\tau = 0.1$ . The entire distributions are plotted in the small boxes against log-scale  $\tau$ .

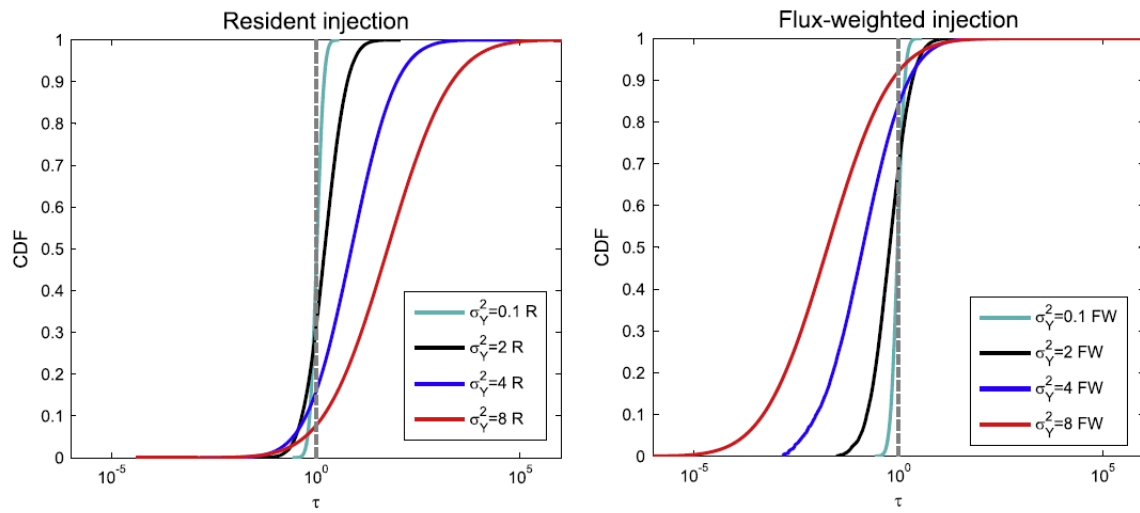
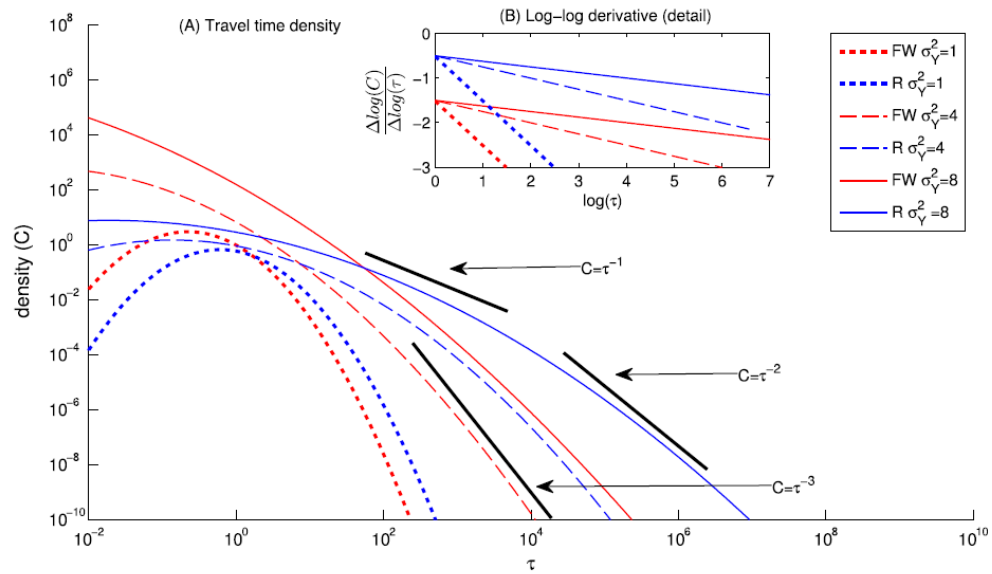


Fig. 3. Travel time cumulative density functions (cdf) for various  $\sigma_Y^2$  versus dimensionless time  $\tau$ , for resident (R) or flux-weighted (FW) injection modes in the ergodic case. The vertical dotted line in gray indicates the distribution for homogeneous case, contrasting with the other heterogeneous ones showing dispersion around their mean value.



**Fig. 4.** Travel time densities ( $C$ ) versus dimensionless time ( $\tau$ ) for different values of  $\sigma_Y^2$ , in double-log axes scales, for both resident (R, blue lines) and flux-weighted (FW, red lines) injection modes in the ergodic case. In the insert, log-log local derivative ( $m = \log(C)/\log(\tau)$ ) versus  $\log(\tau)$ . Black lines are drawn for the visual purpose to indicate apparent PL behaviors with different slopes on the curves. The small box focuses on a portion of the latter plot to make into evidence the region of variability of  $m$  from positive  $\tau$ . (For interpretation of the references to colour in this figure legend, the reader is referred to the web version of this article.)

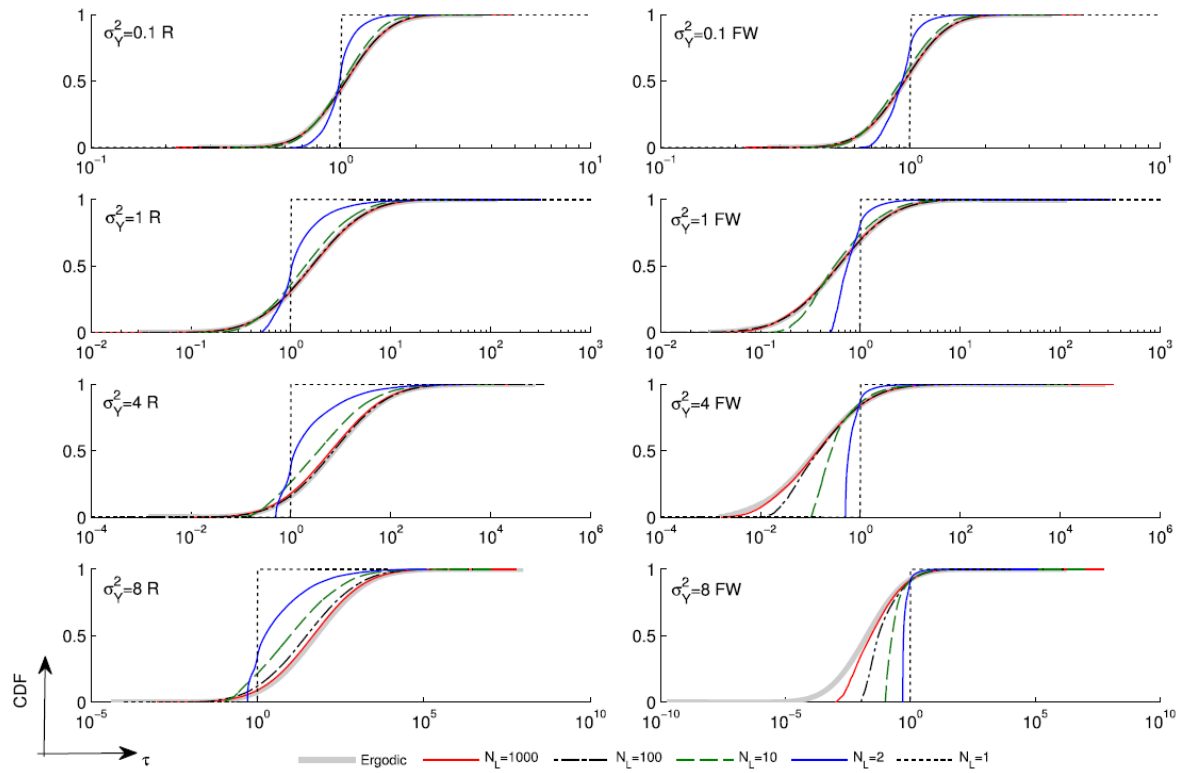
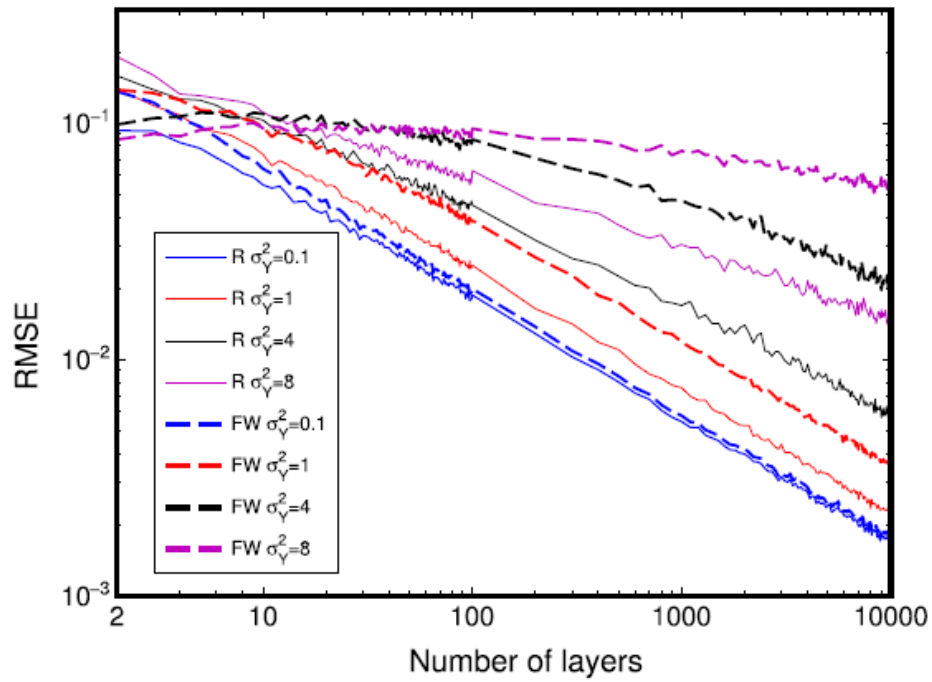


Fig. 5. Ensemble mean behavior of the travel time distribution calculated with 1000 realizations for varying number of layer ( $N_L$ ), variances ( $\sigma_V^2$ ) and type of injection (resident, R, or flux-weighted, FW). The ergodic case (analytical solution) is plotted with a gray line underlying the plots. Note the horizontal scales are very different from case to case, due to the different temporal spreading of the travel time distributions.



**Fig. 6.** Root means square error (RMSE) of the Monte Carlo simulations, indicating the departure from the ensemble mean average, for different varying number on layers ( $N_L$ ), variances of  $Y$  ( $\sigma_Y^2$ ) and type of injection (resident, R, or flux-weighted, FW). The number of realization is constant. For  $\sigma_Y^2 = 0.1$ , a similar behavior is observed both FW and R cases (blue lines); note that for increasing  $\sigma_Y^2$ , FW cases show larger variability, indicating the much more layers need to be added to simulations to reduce the uncertainty in the Monte Carlo estimation. (For interpretation of the references to colour in this figure legend, the reader is referred to the web version of this article.)

### **Acknowledgements**

DP acknowledges the funding provided by the Spanish Ministry of Education through the FPU 2009 PreDoc Program. AF acknowledges funding provided by PRIN 2010–2011 Innovative methods for water resources management under hydro-climatic uncertainty scenarios (2010JHF437).

## References

- [1] Tartakovsky DM, Winter CL. Uncertain future of hydrogeology, ASCE J Hydrol Engrg 2008;13:37-39.
- [2] Dagan G. Flow and Transport in Porous Formations. Berlin: Springer-Verlag; 1989.
- [3] Gelhar LW. Stochastic subsurface hydrology. NJ: Prentice Hall; 1993.
- [4] Rubin Y. Applied stochastic hydrogeology. USA: Oxford University Press; 2003.
- [5] McKenna S, Meigs L, Haggerty R. Tracer tests in a fractured dolomite. 3. doubleporosity, multiple-rate mass transfer processes in convergent flow tracer tests.. Water Resour Res 2001;37:1143-54.
- [6] Fernández-García D, Sánchez-Vila X, Illangasekare TH. Convergent-flow tracer tests in heterogeneous media: combined experimental-numerical analysis for determination of equivalent transport parameters. J Contam Hydrol 2002;57:129-45.
- [7] Fernández-García D, Illangasekare TH, Rajaram H. Conservative and sorptive forced-gradient and uniform flow tracer tests in a three-dimensional laboratory test aquifer. Water Resour Res 2004;40:W10103.
- [8] Ptak T, Piepenbrink M, Martac E. Tracer tests for the investigation of heterogeneous porous media and stochastic modelling of flow and transport - a review of some recent developments. J Hydrol 2004;294:122-63.
- [9] Riva M, Guadagnini A, Fernández-García D, Sánchez-Vila X, Ptak T. Relative importance of geostatistical and transport models in describing heavily tailed breakthrough curves at the Lauswiesen site. J Contam Hydrol 2008;101:1-13.
- [10] Bianchi M, Zheng C, Tick G, Gorelick S. Investigation of small-scale preferential flow with a forced-gradient tracer test. Ground Water 2011;49:503-14.
- [11] Fernández-García D, Rajaram H, Illangasekare TH. Assessment of the predictive capabilities of stochastic theories in a three-dimensional laboratory test aquifer: Effective hydraulic conductivity and temporal moments of breakthrough curves. Water Resour Res 2005;41:W04002.
- [12] Bellin A, Salandin P, Rinaldo A. Simulation and dispersion in heterogeneous porous formation: Statistics, first-order theories, convergence of computations. Water Resour Res 1992;28:2211-27.
- [13] Salandin P, Fiorotto V. Solute transport in highly heterogeneous aquifers. Water Resour Res 1998;34:949-61.
- [14] Jankovic I, Fiori A, Dagan G. Flow and transport in highly heterogeneous formations: 3. Numerical simulations and comparison with theoretical results.

Water Resour Res 2003;39:1270.

[15] Matheron G. Elements Pour Une Theorie des Milieux Poreux. Paris: Masson et Cie; 1967.

[16] Indelman P, Dagan G. Solute transport in divergent radial flow through heterogeneous porous media. J Fluid Mech 1999;384:159-82.

[17] Severino G. Stochastic analysis of well-type flows in randomly heterogeneous porous formations. Water Resour Res 2011;47:W03520.

[18] Severino G, Santini A, Sommella A. Macrodispersion by diverging radial flows in randomly heterogeneous porous media. J Contam Hydrol 2011;123:40-9.

[19] Riva M, Guadagnini A, Ballio F. Time-related capture zones for radial flow in two dimensional randomly heterogeneous media. Stoch Environ Res Risk Assess 1999;13:217-30.

[20] Chao HC, Rajaram H, Illangasekare T. Intermediate-scale experiments and numerical simulations of transport under radial flow in a two-dimensional heterogeneous porous medium. Water Resour Res 2000;36:2869-84.

[21] Pedretti D, Fernández-García D, Bolster D, Sanchez-Vila X. On the formation of heavy-tailed breakthrough curves during convergent flow tracer tests in threedimensional heterogeneous sandy aquifers. Water Resour Res 2013;49:1-17.

[22] Marle C, Simandoux P, Pacsirsky P, Gaulier K. Etude du deplacement fluides miscibles en milieu poreux stratifie. Rev Inst Fr Pet 1967;22:272-94.

[23] Gelhar LW, Gutjahr AL, Naff RL. Stochastic analysis of macrodispersion in a stratified aquifer. Water Resour Res 1979;15:1387-97.

[24] Matheron G, de Marsily G. Is transport in porous media always diffusive? A counterexample. Water Resour Res 1980;16:901-17.

[25] Fiori A, Dagan G. Transport of a passive scalar in a stratified porous medium. Trans Porous Med 2002;47:81-98.

[26] Dentz M, Carrera J. Mixing and spreading in stratified flow. Phys Fluids 2007;19:017107.

[27] Zavala-Sanchez V, Dentz M, Sanchez-Vila X. Characterization of mixing and spreading in a bounded stratified medium. Adv Water Resour 2009;32:635-48.

[28] Bolster D, Valdes-Parada FJ, Le Borgne T, Dentz M, Carrera J. Mixing in confined stratified aquifers. J Contam Hydrol 2011;120-121:198-212.

[29] Jankovic I, Fiori A, Dagan G. Modeling flow and transport in highly heterogeneous three-dimensional aquifers: Ergodicity, Gaussianity, and

anomalous behavior - 1. Conceptual issues and numerical simulations.

Water Resour Res 2006;42:W06D12.

[30] Benson DA, Wheatcraft SW, Meerschaert MM. Application of a fractional advection-dispersion equation. Water Resour Res 2000;36:1403-12.

[31] Haggerty R, McKenna SA, Meigs LC. On the late-time behavior of tracer test breakthrough curves. Water Resour Res 2000;36:3467-79.

[32] Willmann M, Carrera J, Sanchez-Vila X. Transport upscaling in heterogeneous aquifers: What physical parameters control memory functions? Water Resour Res 2008;44:W12437.

[33] Zinn B, Harvey CF. When good statistical models of aquifer heterogeneity go bad: A comparison of flow, dispersion and mass transfer in connected and multivariate gaussian hydraulic conductivity fields. Water Resour Res 2003;39:1051.

[34] Parker JC, Van Genuchten MT. Flux-averaged and volume-averaged concentrations in continuum approaches to solute transport. Water Resour Res 1984;20:866-72.

[35] Kreft A, Zuber A. On the physical meaning of the dispersion equation and its solutions for different initial and boundary conditions. Chem Eng Sci 1978;33:1471-80.

[36] Demmy G, Berglund S, Graham W. Injection mode implications for solute transport in porous media: Analysis in a stochastic lagrangian framework. Water Resour Res 1999;35:1965-73.

[37] Frampton A, Cvetkovic V. Significance of injection modes and heterogeneity on spatial and temporal dispersion of advecting particles in two-dimensional discrete fracture networks. Adv Water Resour 2010;32:649-58.

[38] Jankovic I, Fiori A. Analysis of the impact of injection mode in transport through strongly heterogeneous aquifers. Adv Water Resour 2010;33:1199-205.

[39] Bear J. Hydraulics of groundwater. McGraw-Hill International Book Co., 1979.

[40] Shvidler MI. The source-type solution of the problem of unsteady flow in random porous media (in Russian). Izv Akad Nauk USSR Mekh Zhidk Gaza 1966;4:137.

[41] Indelman P, Fiori A, Dagan G. Steady flow toward wells in heterogeneous formations: Mean head and equivalent conductivity. Water Resour Res 1996;32:1975-83.

[42] Moench A. Convergent Radial Dispersion: A Laplace Transform Solution for

Aquifer Tracer Testing. *Water Resour Res* 1989;25:439-47.

[43] Freeze RA. A stochastic-conceptual analysis of one-dimensional groundwater flow in nonuniform homogeneous media. *Water Resour Res* 1975;11:725-41.

[44] Aitchison J, Brown JAC. *The Lognormal Distribution, with Special Reference to Its Use in Economics*. New York: Cambridge University Press; 1957.

[45] Crow EL, Shimizu K, editors. *Lognormal Distributions: Theory and Applications*. New York: Dekker; 1988.

[46] Bouchaud JP, Georges A. Anomalous diffusion in disordered media-statistical mechanisms, models and physical applications. *Phys Rep* 1990;195:127-293.

[47] Bohling GC, Liu G, Knobbe SJ, Reboulet EC, Hyndman DW, Dietrich P, Butler JJ. Geostatistical analysis of centimeter-scale hydraulic conductivity variations at the MADE site, *Water Resour Res* 2012;48:W02525.

[48] de Barros FPJ, Rubin Y. A risk-driven approach for subsurface site characterization. *Water Resour Res* 2008;58:W01414.

[49] Bolster D, Barahona-Palomo M, Dentz M, Garcia DF, Sanchez-Vila X, Trinchero P, Valhondo C, Tartakovsky DM. Probabilistic risk assessment applied to contamination scenarios in porous media. *Water Resour Res* 2009;45:W06413.

[50] Clauset A, Shalizi CR, Newman ME. Power-law distribution in empirical data. *SIAM Rev* 2007;51:661-703.

[51] Gouze P, Le Borgne T, Leprovost R, Lods G, Poidras T, Pezard P. Non-Fickian dispersion in porous media: 1. Multiscale measurements using single-well injection withdrawal tracer tests. *Water Resour Res* 2008;44:W06426.

[52] Pedretti D, Fernández-García D. A locally-adaptive and automatic method to estimate heavily-tailed breakthrough curves from particle distributions. *Adv Water Resour* 2013;59:52-65.